arXiv:1603.04377v1 [cond-mat.str-el] 14 Mar 2016

Double-phase transition and giant positive magnetoresistance in the quasi-skutterudite $Gd_3Ir_4Sn_{13}$

Harikrishnan S. Nair,[1, a)] Sarit K. Ghosh[‡],[1, 2] Ramesh Kumar K.,[1] and André M. Strydom[1, 3, 4]

[1)] *Highly Correlated Matter Research Group, Physics Department, P. O. Box 524, University of Johannesburg, Auckland Park 2006, South Africa*

[2)] *Department of Applied Physics, Birla Institute of Technology, Mesra 835215, Ranchi, Jharkhand, India*

[3)] *Institute of Physics, Chinese Academy of Sciences, PO Box 623, Beijing 100190, China*

[4)] *Max Planck Institute for Chemical Physics of Solids (MPICPfS), Nöthnitzerstraße 40, 01187 Dresden, Germany*

(Dated: 15 March 2016)

The magnetic, thermodynamic and electrical/thermal transport properties of the caged-structure quasi-skutterudite $Gd_3Ir_4Sn_{13}$ are re-investigated. The magnetization $M(T)$, specific heat $C_p(T)$ and the resistivity $\rho(T)$ reveal a double-phase transition – at $T_{N1} \sim 10$ K and at $T_{N2} \sim 8.8$ K – which was not observed in the previous report on this compound. The antiferromagnetic transition is also visible in the thermal transport data, thereby suggesting a close connection between the electronic and lattice degrees of freedom in this Sn-based quasi-skutterudite. The temperature dependence of $\rho(T)$ is analyzed in terms of a power-law for resistivity pertinent to Fermi liquid picture. Giant, positive magnetoresistance (MR) $\approx 80\%$ is observed in $Gd_3Ir_4Sn_{13}$ at 2 K with the application of 9 T. The giant MR and the double magnetic transition can be attributed to the quasi-cages and layered antiferromagnetic structure of $Gd_3Ir_4Sn_{13}$ vulnerable to structural distortions and/or dipolar or spin-reorientation effects. The giant value of MR observed in this class of 3:4:13 type alloys, especially in a Gd-compound, is the highlight of this work.

[a)] Electronic mail: h.nair.kris@gmail.com

I. INTRODUCTION

$R_3T_4X_{13}$ are caged structure compounds in the class of strongly correlated electron intermetallics where, R is either a rare-earth element, an early d-block element such as Sc or Y, or the alkali-earth metals Ca or Sr. T stands for a Group VIII d-electron element, and X is either In, Ge, or Sn. The $R_3T_4X_{13}$ compounds crystallize in the cubic space group $Pm\overline{3}n$. Remeika *et al.*[1] were the first to report on $R_3T_4X_{13}$ phases but, the literature refers to the archetypal $R_3T_4X_{13}$ phase as either the $Pr_3Rh_4Sn_{13}$-structure type[2], or the $Yb_3Rh_4Sn_{13}$-type[3]. This structure type allows a single crystallographic site for occupation by each of the R and T atoms, and two distinct sites are available to the X atom. A schematic of the crystal structure is presented in Fig 1 showing the cage-like structural network. $R_3T_4X_{13}$ attracted attention mainly due to the discovery of superconductivity with superconducting temperatures as high as $T_{sc} = 8$ K in $Yb_3Rh_4Sn_{13}$ and $Ca_3Rh_4Sn_{13}$[1] but this structure-type has been of enduring interest due to its amenability to many different elements and the wide variety of physical properties.[4,5] Remeika *et al.,* reported the crystal structure of $R_3T_4X_{13}$ in a cubic primitive unit cell,[1] however, also suggested face-centered and tetragonal structures as possible unit cells. Hodeau *et al.,* reported a body-centered unit cell for the same class of compounds.[6] Modifications to the cubic structure with changes in stoichiometry were suggested in Ref.[7].[7] The first two reports on the crystal structure of the germanides are from Segre *et al.,*[8] and from Bruskov *et al.,*[9] who proposed a disordered variant of the crystal structure where Ge atoms partially occupy two different $24k$ sites. A positional disorder of the X atom or the formation of random mixture of R/T and X atoms are known.[10,11] Doubling of the unit cell has been observed with a non-centrosymmetric $I4_132$ space group in some of the stannides (X = Sn) of $R_3T_4X_{13}$.[12,13]

Stannides (X = Sn) in this class have been investigated in some detail, for example, $Ce_3Ir_4Sn_{13}$[14] and $Ce_3Rh_4Sn_{13}$[15] are classified as heavy-fermion systems where high effective mass or larger density of states at the Fermi level have been observed. The stannide-$R_3T_4X_{13}$ display superconductivity in the case of $R_3Rh_4Sn_{13}$ (for R = La, Yb, Ca, Sr, Th) while antiferromagnetism for Gd and Eu.[6] A double-magnetic phase transition at 0.6 K and 2.1 K is exhibited by the Ce-based stannide, $Ce_3Ir_4Sn_{13}$.[16] On the other hand, $Eu_3Ir_4Sn_{13}$ where Eu shows valence fluctuation between non-magnetic Eu^{3+} ($4f^6$) and magnetic Eu^{2+} ($4f^7$), shows an antiferromagnetic phase transition at 10 K.[17] Nagoshi *et al.,* studied single crystals

of $Gd_3Ir_4Sn_{13}$ using magnetic susceptibility, resistivity, Hall effect and epithermal neutron scattering.[12] They identified a structural distortion characterized by the propagation vector (1/2, 1/2, 0). Only a single magnetic transition was identified at 10 K from macroscopic measurements. The magnetic moment direction of Gd in the ordered state is suggested to be perpendicular to the chain axis in each magnetic sublattice.[12] Antiferromagnetic interactions in one-dimensional chains together with ferromagnetic interaction between the nearest chains in the same sublattice was assumed to be the reason behind the phase transition at 10 K. $R_3X_4Sn_{13}$ compounds have been, in fact, reported to display multiple phase transitions in close temperature intervals. For example, $Eu_3Ir_4Sn_{13}$ is reported to show two transitions in resistivity and specific heat occurring at $T^* \sim 57$ K and at $T_N \approx 10$ K.[17,18] The transition at T^* was attributed to a structural distortion due to the displacement of Sn ions in the $Sn(1)Sn(2)_{12}$ cages while the transition at T_N was attributed to antiferromagnetic ordering. Interestingly, the structural distortion and the antiferromagnetic ordering were characterized by the same propagation vector, $\mathbf{q_c} = (1/2, 1/2, 0)$.[19] Eventhough the structural transition at T^* was observed to be suppressed by the application of external pressure up to 10.3 kbar, the magnetic transition was not affected.[18] With the application of magnetic field, a new feature was observed to develop in the magnetically ordered state. Anomalous phase transitions were observed in $Ce_3Ir_4Sn_{13}$ as well, where the anomalies occurred at 0.6 K and at 2 K.[16] The transition at 0.6 K was identified as antiferromagnetic whereas the one at 2 K was argued to be due to a change of band structure accompanied by a lattice expansion. Interestingly, magnetic susceptibility did not present an anomaly at 2 K. It must be noted here that an earlier report on $Ce_3Ir_4Sn_{13}$ had shown that the 2 K-transition split into a very sharp peak at 2.10 K and a shoulder-like one at 2.18 K.[20] A closely related compound, $Eu_3Rh_4Sn_{13}$, showed only one anomaly at 11.2 K due to an antiferromagnetic transition[21] but, in the magnetization measured for $H \parallel [110]$ it showed two close-by transition when the applied field was 13 T. While the previous report[17] speculated on the possibility of polaronic effects via electron-phonon coupling or Fermi surface induced changes in the conduction electrons scattering to be the origin of the transition at T^*, present understanding[18] attributes the origin of the high temperature transition to structural disorder within the cages.

In the present paper we endeavor to re-investigate $Gd_3Ir_4Sn_{13}$ using magnetization, specific heat and electrical resistivity measurements on a polycrystalline sample. Even though a polycrystalline sample was used for the study, two very close-by magnetic transitions in

$Gd_3Ir_4Sn_{13}$ are identified through high resolution measurements. In addition, giant, positive MR $\approx 80\%$ is observed in this compound at 2 K which, to the best of our knowledge, is the highest reported so far in this class of Gd-compounds.

II. EXPERIMENTAL DETAILS

Polycrystalline samples of $Gd_3Ir_4Sn_{13}$ were prepared by arc melting the constituent elements Gd (99.99%), Ir (-22 mesh, Premion 99.99% Alfa Aesar) and Sn (99.99% Alfa Aesar) together. The elements weighed according to stoichiometric ratio were melted in the water-cooled Cu-hearth of Edmund Buehler arc melting furnace under static atmosphere of purified argon gas. A Zr-getter trap was used for purifying the Ar gas. The once-melted sample was flipped over and re-melted 5 times in order to ensure a single homogeneous phase. The melted samples were annealed for 2 weeks at 680 °C. Powder X ray diffractogram of pulverized sample of $Gd_3Ir_4Sn_{13}$ was obtained using a Philips X'pert diffractometer using Cu-Kα radiation. Structural analysis of the x ray diffraction data was performed using Rietveld method[22] implemented in FullProf suite of programs.[23] Magnetic measurements were performed using a commercial Magnetic Property Measurement System (MPMS) and specific heat was measured using a commercial Physical Property Measurement System (PPMS) (both instruments from Quantum Design, San Diego). Electrical resistivity was measured on a bar-shaped sample of dimension $l \times b \times \phi \approx 5$ mm $\times$ 3 mm $\times$ 0.8 mm using the ac transport option of the PPMS. For magnetoresistance measurements, the magnetic field B, the current I, and sample length l were arranged such that $B \perp I \parallel l$. Thermal conductivity and Seebeck coefficients were measured on a bar shaped sample using the Thermal Transport Option (TTO) of the PPMS.

III. RESULTS

A. Crystal structure & distortions

The crystal structure of $R_3T_4X_{13}$ compounds is generally described in cubic $Pm\overline{3}n$ space group (#223). Recent crystallography work on $R_3T_4X_{13}$[24] compounds point towards the existence of subtle structural distortions in this class of compounds and confirms the findings of earlier reports.[1,2,6,25] Rietveld refinement of the x ray data on $Gd_3Ir_4Sn_{13}$ was performed

using the $Pm\bar{3}n$ space group. The results of the refinement are presented in Fig 2 where the experimentally observed data are shown in circles and the calculated pattern as thick solid line. The refinement yielded a lattice parameter value of a (Å) = 9.6539(3). Nagoshi *et al.*,[12] pointed out the presence of several extra reflections mainly in the 2θ range of 25 to 55° in the x ray diffraction pattern obtained on a single crystal of $Gd_3Ir_4Sn_{13}$. A close inspection of the x ray diffractogram of our sample also revealed additional superstructure peaks signifying structural distortions in the present sample of $Gd_3Ir_4Sn_{13}$. The (2θ, (h, k, l)) pairs of the peaks are as following: (31.5°, $(1/2, 3/2, 3)$), (37.9°, $(1/2, 7/2, 2)$), (44.5°, $(5/2, 7/2, 2)$) and (50.5°, $(7/2, 7/2, 2)$). One such peak is shown enlarged in the inset of Fig 2 where the intensity is scaled down by a factor of 10^4. These peaks are indexed following the structural distortion with a propagation vector $\mathbf{q_c}$ = (1/2, 1/2, 0) (a minor impurity belonging to βSn was observed at 43°). The distorted structure of this type can be assigned to the space group $I4_132$, similar to the superlattice structure for $Gd_3Rh_4Sn_{13}$ and $La_3Rh_4Sn_{13}$.[25]

B. Specific heat

The experimentally measured specific heat, $C_p(T)$, of $Gd_3Ir_4Sn_{13}$ is presented in the panel (a) of Fig 3 along with that of the non-magnetic analogue $La_3Ir_4Sn_{13}$ which is shown in the figure using a solid line. The Dulong-Petit value of $3nR \approx 166$ J/mol.Gd-K is recovered for $Gd_3Ir_4Sn_{13}$ at 300 K (n is 1/3 of the number of atoms in the formula unit and R is the universal gas constant). The $C_p(T)$ of $Gd_3Ir_4Sn_{13}$ resembles that of other $R_3T_4X_{13}$ compounds reported in the literature.[26,27] However, the low-temperature region of specific heat gives evidence of a double magnetic phase transition with two nearby peaks at $T_{N1} \approx$ 10 K and $T_{N2} \approx 8.8$ K. The inset of Fig 3 magnifies the temperature region between 1 K and 14 K to highlight the double-peaks. Presented in the panel (b) are the specific heat data under applied magnetic fields of 4 T and 9 T. It is observed that the application of magnetic field shifts the peak at $T_{N1} \approx 10$ K to low temperatures. Previous report on the magnetic and transport properties of $Gd_3Ir_4Sn_{13}$ did not identify the signature of double magnetic phase transition in their data.[12] The magnetic entropy, $S_m(T)$, was estimated by subtracting the specific heat of non-magnetic analogous compound $La_3Ir_4Sn_{13}$ from that of $Gd_3Ir_4Sn_{13}$. In this way, $S_m \sim$17.2 J/mol-K was obtained at T_{N1} which is equal to $R\ln(8)$ for the full multiplet of Gd^{3+} ($S_m \approx$16 J/mol-K, at T_{N2}).

C. Magnetization

The inverse magnetic susceptibility, $1/\chi(T)$, of $Gd_3Ir_4Sn_{13}$ at 500 Oe is presented in the panel (a) of Fig 4. A curve-fit assuming Curie-Weiss law performed in the range 80–300 K is shown as a straight line. The Curie-Weiss fit leads to a value of effective paramagnetic moment $\mu_{\rm eff}$ = 7.2 $\mu_{\rm B}$/Gd-atom and Curie temperature $\theta_{\rm CW}$ = -21 K. The $\theta_{\rm CW}$ and $\mu_{\rm eff}$ values are comparable to the theoretical free-ion value for Gd^{3+}, $\approx$ 7.94 $\mu_{\rm B}$/ Gd-atom. The observed deviation of the experimental value of magnetic moment from that of the free ion Gd is interesting and might hint at the contributions from $5d$ electrons. The double-transition in $Gd_3Ir_4Sn_{13}$ is evident in magnetic response seen in the panel (b) of Fig 4, where $M(T)$ in zero field cooled cycle measured at 500 Oe is presented in enlarged scales. The panel (c) of Fig 4 shows the magnetization isotherms, $M(H)$ at 2.5 K and at 10 K plotted together. No signature of ferromagnetism or metamagnetism is observed in the magnetization isotherms while up to 9 T, the antiferromagnetic behaviour is retained.

D. Resistivity and magnetoresistance

The electrical resistivity, $\rho(T)$, of $Gd_3Ir_4Sn_{13}$ in 0 T is presented in the main panel of Fig 5. In general, a metal-like behaviour is observed with a prominent anomaly at $\approx$ 10 K. This "kink" corresponds to T_{N1}. The residual resistance ratio (RRR) defined as $\rho(300\ K)/\rho(2\ K)$ is approximately 50, which is higher than the value of RRR = 3 obtained on $Gd_3Ir_4Sn_{13}$ single crystals.[12] This difference between our data and that of Nagoshi *et al.,* is large only in the magnetic state. Above the transition temperature the ratios are comparable. The deviation from the RRR of a single crystal could possibly be due to a combination of grain boundary effects and electron-phonon scattering at high temperature. The Mott term also could be relevant because the variation becomes non-linear at relatively low temperature which is a signature of *s*-*d* interband scattering. Enhanced quality of the polycrystalline samples reflected in RRR and visibility of low-temperature transition were observed in $Ce_3Pd_{20}Si_6$ for example.[28] A closer inspection of the temperature derivative dρ/dT plotted in the inset (a) brings up both the anomalies T_{N1} and T_{N2} clearly. It is observed that the electrical

resistivity of $Gd_3Ir_4Sn_{13}$ below the transition at T_{N1} can be faithfully described by the expression;

$$\rho(T) = \rho_0 + AT^n \tag{1}$$

In this expression, the first term accounts for impurity scattering. A power-law of the form AT^n accounts for the normal Fermi-liquid quasiparticle excitation where $1 < n < 2$. During the fit, the exponent n was left as a free parameter yielding a value of $n \approx 1.52(2)$ for 0 T while it gradually increased to 1.63(2) for 9 T. The parameters derived from the fit are collected in Table I.

The magnetoresistance, defined as $\mathrm{MR}\% = \frac{\rho(H)-\rho(H=0)}{\rho(H=0)} \times 100$, of $Gd_3Ir_4Sn_{13}$ is plotted in the main panel of Fig 6. The MR is calculated for $H = 1$, 4 and 9 T. As can be seen from the figure, with the application of 9 T giant, positive MR $\approx 80\%$ is obtained at 2 K. A progressive increase of MR with applied magnetic field can be observed. What is evident is the sudden increase of MR at T_{N1} suggesting a close connection between the appearance of MR and the antiferromagnetic transition. Above $T_{N1} \approx 10$ K, the magnetoresistance is nearly zero for any value of applied field. In the inset of Fig 6, the isothermal magnetoresistance is plotted for 2 K and for 15 K. The positive MR is clearly reproduced for the isotherm at 2 K whereas at 15 K, a linear behaviour is recovered.

E. Thermal transport

The experimentally measured thermal conductivity of $Gd_3Ir_4Sn_{13}$ is presented in the main panel of Fig 7 (a) denoted as κ_{T}. The electronic contribution to the total thermal conductivity is estimated using the Wiedemann -Franz law as $\kappa_{\mathrm{e}} = \frac{L_0 T}{\rho(T)}$. The Lorenz number is $L_0 = \left(\frac{\pi k_B^2}{e\sqrt{3}}\right)^2 = 2.54 \times 10^{-8}\ \mathrm{W\Omega K^{-2}}$ and $\rho(T)$ is the electrical resistivity. The κ_{e} estimated this way is subtracted from the total thermal conductivity to obtain the phonon contribution, κ_{ph} ($\kappa_T(\mathrm{T}) = \kappa_{\mathrm{e}}(T) + \kappa_{\mathrm{ph}}(T)$). Both κ_{e} and κ_{ph} are shown in Fig 7. It is interesting to note that the magnetic transition at T_{N1} is clearly reflected in the thermal conductivity data. The thermal conductivity data bears a resemblance to the thermal transport data of other quasi-skutterudite compounds like $Y_3Ir_4Ge_{13}$.[26] However, the thermopower of $Gd_3Ir_4Sn_{13}$ exhibits a behaviour slightly different from that of the Ge-based compounds of this class.[15,26,27] A plateau-like region in the thermopower seen in the Ge-based compounds is not seen in the present case, instead, a linear increase of thermopower is observed.

IV. DISCUSSION

The phase transitions T^* and T_N reported to be observed in the stannides were not as close-by in temperature as has been observed as T_{N1} and T_{N2} in $Gd_3Ir_4Sn_{13}$ (*i.e.,* at 8.8 K and 10 K). The double-transition in the present compound is observed in $M(T)$, $C_P(T)$, $\rho(T)$ and in thermal conductivity and hence is a intrinsic bulk effect. At lower applied fields like 500 Oe, both the transitions T_{N1} and T_{N2} are clearly observed in the $M(T)$ curve (see Fig 4). When the applied field increases, the transition at T_{N2} becomes less conspicuous in $M(T)$, but is still clearly identified in d$M(T)$/dT. It is noted that with applied field, the T_{N1} shifts to lower temperature while that at T_{N2} remains unaffected. Such a feature is also reflected in the specific heat. The earlier report on single crystals of $Gd_3Ir_4Sn_{13}$ proposed a chain-like magnetic structure for this compound with interlayer antiferromagnetic coupling and weak ferromagnetism between the layers.[12] In order to test whether any presence of ferromagnetism can be detected, we performed ac susceptibility measurements (data not shown here). Though signs of both T_{N1} and T_{N2} were clear in the data, there was no frequency dispersion present. Also, the imaginary part of the ac susceptibility did not show any temperature dependence ruling out any dissipative or ferromagnetic terms. The type of antiferromagnetic order in Gd-alloys can be inferred from scrutinizing the specific heat.[30,31] The peak value of magnetic specific heat at the transition temperature is estimated to be 20.15 J/mol K if the magnetic structure is any equal moment structure like simple antiferro-, ferro- or heli-magnetic. Any amplitude modulation is expected to reduce this value. In the present case of $Gd_3Ir_4Sn_{13}$, a non-collinear magnetic structure may be expected following this test. Amplitude modulated magnetic structures are very common among highly anisotropic rare earth compounds with orbital magnetism. However, Gd is a S-state ion with $L = 0$ and hence one could assume that dipolar interactions can become relevant as has been reported in several Gd-compounds.[32] It is interesting to note also that the J-J coupling scheme becomes relevant in the case where Hund's coupling is modest compared to the spin-orbit coupling and it was shown by Niikura *et al.,* that one of the seven $4f$ electrons of Gd can result in carrying a quadrupole moment.[33]

The observation of positive giant magnetoresistance in $Gd_3Ir_4Sn_{13}$, is an important finding of the present work. The $R_3X_4Sn_{13}$ compounds are not reported to exhibit giant or positive magnetoresistance. However, magnetoresistance anomalies in Gd-alloys have been

studied in detail and documented well.[34–39] It is interesting to note that the temperature dependence of electrical resistivity of Gd-alloys like $GdCu_2Si_2$ and $GdNi_2Si_2$ resemble that of $Gd_3Ir_4Sn_{13}$.[34] The MR is observed to be positive for $GdCu_2Si_2$ above the Néel temperature.[34] This observation suggested that the contribution from the paramagnetic Gd fluctuation is small compared to that from the influence of magnetic field on the Fermi surface. On the other hand, for the Ni-based alloy, the MR is negative in the paramagnetic state. Though this feature is reminiscent of Kondo spin fluctuation phenomena, since Gd f electrons are well-localized, this feature is attributed to the spin fluctuations from the Ni d-band. In contrast to these two features, the MR of $Gd_3Ir_4Sn_{13}$ is temperature independent at 15 K which is above T_{N1}. From the analysis of effective paramagnetic moment, it was seen that possible contributions from the $5d$ electrons are present in $Gd_3Ir_4Sn_{13}$. $Gd_2Ni_3Si_5$ is another compound that is reported to exhibit positive giant magnetoresistance.[38] However, the MR was not correlated to the rare earth moments but to the magnetic ordering of the lattice as the magnitude of MR is found to be significantly reduced in the paramagnetic state. Notably, the MR was observed to be large in non-magnetic rare earths other than Gd in $R_2Ni_3Si_5$ ($Gd_2Ni_3Si_5$ showed $\approx 12\%$ at 4.4 K for 45 kOe).[38] In $Gd_3Ir_4Sn_{13}$ also the enhancement of MR is prominent below the magnetic ordering temperature which hints at the connection between magnetic ordering and giant MR. Similar to $Gd_3Ir_4Sn_{13}$, $Gd_2Ni_3Si_5$ also has a layered magnetic structure and this structural feature also might play a role in the high value of MR. On the other hand, giant magnetoresistance observed in Gd-based magnetocaloric alloys like $Gd_5(Si_{1.8}Ge_{2.2})$[36] is attributed to the presence of first-order magnetostructural transition. Note that in this compound a negative MR was observed. A similar feature was observed in Ge-rich compound $Gd_5(Si_{0.1}Ge_{0.9})_4$.[37]

Usually, positive MR can arise from Lorentz contribution to resistivity. In pure metals, high cyclotron frequency and relaxation times can lead to positive MR. However, such a scenario does not hold in the case of $Gd_3Ir_4Sn_{13}$ which shows a higher low temperature resistivity than pure metals. Another possibility is for positive MR in antiferromagnets to arise due to enhancement of spin fluctuations.[40] However, MR in such case is not as high as been observed in $Gd_3Ir_4Sn_{13}$. Gd-ion being an S-state ion, crystalline electric field effects can be ruled out as reasons for the observed giant MR. At this point it is interesting to mention that the discovery of giant magnetoresistance was made on layered magnetic structures with antiferromagnetic interlayer exchange.[41] A highly plausible reason for the double-magnetic

transition and the positive giant magnetoresistance could be spin-reorientation effects taking place in the layered magnetic structure of $Gd_3Ir_4Sn_{13}$ with interlayer antiferromagnetic exchange.[12] However, it must be noted that spin-reorientation effects in $Tb_2Ni_3Si_5$ was evident in isothermal magnetization plots at 6 K and consequently was argued to have lead to positive giant MR.[38] The magnetization isotherms of $Gd_3Ir_4Sn_{13}$ at 2.5 K (Fig 4 (b)) do not present any deviation from linearity to support effects of spin-reorientation.

V. CONCLUSIONS

The double-phase transition in the quasi-skutterudite $Gd_3Ir_4Sn_{13}$ is unambiguously identified through magnetization, specific heat, electrical resistivity, and thermal conductivity measurements. The two transitions occur very close to each other at $T_{N1} \approx 10$ K and at $T_{N2} \approx 8.8$ K. The transition at T_{N1} is seen to shift to lower temperature with application of magnetic field hence, revealing the antiferromagnetic nature whereas the transition at 8.8 K is very robust and does not change upon applied field. The interesting result is the observation of positive giant magnetoresiatance of about 80% below T_{N1}. The layered quasi-1D magnetic structure of $Gd_3Ir_4Sn_{13}$ and/or dipolar interactions commonly found in Gd-based antiferromagnets could be the reason for the double-magnetic transition and the positive giant magnetoresisatnce.

‡Present address: Department of Applied Physics, Birla Institute of Technology, Mesra, Ranchi, Jharkhand, India

HSN and RKK acknowledge FRC/URC of UJ for postdoctoral fellowship. AMS thanks the SA NRF (93549) and UJ URC/FRC for financial assistance.

REFERENCES

[1]J. P. Remeika, G. P. Espinosa, A. S. Cooper, H. Barz, J. M. Rowell, D. B. McWhan, J. M. Vandenberg, D. E. Moncton, Z. Fisk, L. D. Woolf, *et al.*, Solid State Commun. **34**, 923 (1980).

[2]J. M. Vandenberg, Mater. Res. Bull. **15**, 835 (1980).

[3]J. L. Hodeau, J. Chenavas, M. Marezio, and J. P. Remeika, Solid State Commun. **36**, 839 (1980).

[4]N. Kase, H. Hayamizu, K. Inoue, and J. Akimitsu, Physica C **471**, 711 (2011).

[5]P. D. Kulkarni, S. S. Banerjee, C. V. Tomy, G. Balakrishnan, D. M. Paul, S. Ramakrishnan, and A. K. Grover, Phys. Rev. B **84**, 014501 (2011).

[6]J. L. Hodeau, M. Marezio, J. P. Remeika, and C. H. Chen, Solid State Commun. **42**, 97 (1982).

[7]B. Eisenmann and H. Schäfer, J. Less Comm. Metals **123**, 89 (1986).

[8]C. U. Segre, H. F. Braun, and K. Yvon, Ternary Superconductors , 243 (1981), ed. G. K. Shenoy.

[9]V. A. Bruskov, V. K. Pecharskij, and O. I. Bodak, Izv. Akad. Nauk. SSSR Neorg. Mater. **22**, 1471 (1986).

[10]Y. Mudryk, A. Grytsiv, P. Rogl, C. Dusek, A. Galatanu, E. Idl, H. Michor, E. Bauer, C. Godart, D. Kaczorowski, *et al.*, J. Phys.: Condens. Matter **13**, 7391 (2001).

[11]D. Niepmann, R. Pöttgen, K. M. Poduska, F. J. DiSalvo, H. Trill, and B. D. Mosel, Z Natur. **56b**, 1 (2001).

[12]C. Nagoshi, R. Yamamoto, K. Kuwahara, H. Sagayama, D. Kawana, M. Kohgi, H. Sugawara, Y. Aoki, H. Sato, T. Yokoo, *et al.*, J. Phys. Soc. Jpn. **75**, 044710 (2006).

[13]P. Bordet, D. E. Cox, G. P. Espinosa, J. L. Hodeau, and M. Marezio, Solid State Commun. **78**, 359 (1991).

[14]H. Sato, T. Fukuhara, S. Iwakawa, Y. Aoki, I. Sakamoto, S. Takayanagi, and N. Wada, Physica B **186**, 630 (1993).

[15]U. Köhler, A. P. Pikul, N. Oeschler, T. Westerkamp, A. M. Strydom, and F. Steglich, J. Phys.: Condens. Matter **19**, 386207 (2007).

[16]C. Nagoshi, H. Sugawara, Y. Aoki, S. Sakai, M. Kohgi, H. Sato, T. Onimaru, and T. Sakakibara, Physica B **359**, 248 (2005).

[17]L. Mendonça-Ferreira, E. M. Bittar, M. A. Pires, R. R. Urbano, O. Agüero, I. Torriani, C. Rettori, P. G. Pagliuso, A. Malachias, E. Granado, *et al.*, Physica B **384**, 332 (2006).

[18]L. Mendonça-Ferreira, E. M. Bittar, I. K. E. Bianchi, P. F. S. Rosa, Z. Fisk, and P. G. Pagliuso, in *J. Phys.: Conf. Ser.*, Vol. 592 (IOP Publishing, 2015) p. 012046.

[19]J. R. L. Mardegan, N. Aliouane, L. N. Coelho, O. Aguero, E. M. Bittar, J. C. Lang, P. G. Pagliuso, I. L. Torriani, and C. Giles, IEEE Transactions on Magnetics **49**, 4652 (2013).

[20]S. Takayanagi, H. Sato, T. Fukuhara, and N. Wada, Physica B **199**, 49 (1994).

[21]A. Maurya, P. Bonville, A. Thamizhavel, and S. K. Dhar, JPS Conf. Proc. **3**, 017022 (2014).

[22]H. M. Rietveld, J. Appl. Cryst. **2**, 65 (1969).

[23]J. Rodriguez-Carvajal, Physica B **192**, 55 (1993).

[24]R. Gumeniuk, L. Akselrud, K. O. Kvashnina, W. Schnelle, A. A. Tsirlin, C. Curfs, H. Rosner, M. Schöneich, U. Burkhardt, U. Schwarz, *et al.*, Dalton Trans. **41**, 6299 (2012).

[25]S. Miraglia, J. L. Hodeau, M. Marezio, C. Laviron, M. Ghedira, and G. P. Espinosa, J. Solid State Chem. **63**, 358 (1986).

[26]A. M. Strydom, J. Phys.: Condens. Matter **19**, 386205 (2007).

[27]A. M. Strydom, N. Oeschler, and F. Steglich, Physica B **403**, 746 (2008).

[28]A. Prokofiev, J. Custers, M. Kriegisch, S. Laumann, M. Müller, H. Sassik, R. Svagera, M. Waas, K. Neumaier, A. M. Strydom, *et al.*, Phys. Rev. B **80**, 235107 (2009).

[29]P. d. V. du Plessis, A. M. Strydom, R. Troc, T. Cichorek, C. Marucha, and R. P. Gers, J. Phys.: Condens. Matter **11**, 9775 (1999).

[30]M. Bouvier, P. Lethuillier, and D. Schmitt, Phys. Rev. B **43**, 13137 (1991).

[31]J. A. Blanco, D. Gignoux, and D. Schmitt, Phys. Rev. B **43**, 13145 (1991).

[32]M. Rotter, M. Loewenhaupt, M. Doerr, A. Lindbaum, H. Sassik, K. Ziebeck, and B. Beuneu, Phys. Rev. B **68**, 144418 (2003).

[33]F. Niikura and T. Hotta, J. Phys. Soc. Jpn. **81**, 114720 (2012).

[34]E. V. Sampathkumaran and I. Das, Phys. Rev. B **51**, 8631 (1995).

[35]R. Mallik and E. V. Sampathkumaran, Phys. Rev. B **58**, 9178 (1998).

[36]L. Morellon, J. Stankiewicz, B. Garcia-Landa, P. A. Algarabel, and M. R. Ibarra, Appl. Phys. Lett. **73**, 3462 (1998).

[37]L. Morellon, P. A. Algarabel, C. Magen, and M. R. Ibarra, J. Magn. Magn. Mater. **237**, 119 (2001).

[38]C. Mazumdar, A. K. Nigam, R. Nagarajan, C. Godart, L. C. Gupta, B. D. Padalia, G. Chandra, and R. Vijayaraghavan, Appl. Phys. Lett. **68**, 3647 (1996).

[39]C. Mazumdar, K. Ghosh, R. Nagarajan, S. Ramakrishnan, B. D. Padalia, and L. C. Gupta, Phys. Rev. B **59**, 4215 (1999).

[40]H. Yamada and S. Takada, Prog. Theor. Phys. **49**, 1401 (1973).

[41]G. Binasch, P. Grünberg, F. Saurenbach, and W. Zinn, Phys. Rev. B **39**, 4828 (1989).

TABLE I. The parameters extracted from the curve-fit to electrical resistivity $\rho(T)$ of $Gd_3Ir_4Sn_{13}$ under different values of applied magnetic fields, H_{app}, assuming Eqn (1) for resistivity behaviour under Fermi liquid picture.

H_{app} (Tesla)	0	1	4	9
ρ_0 ($\mu\Omega$cm)	28.9	31.1	42.7	60.6
A ($\mu\Omega$cm/ K^2)	2.12	1.99	1.63	1.20
n	1.52	1.53	1.58	1.63

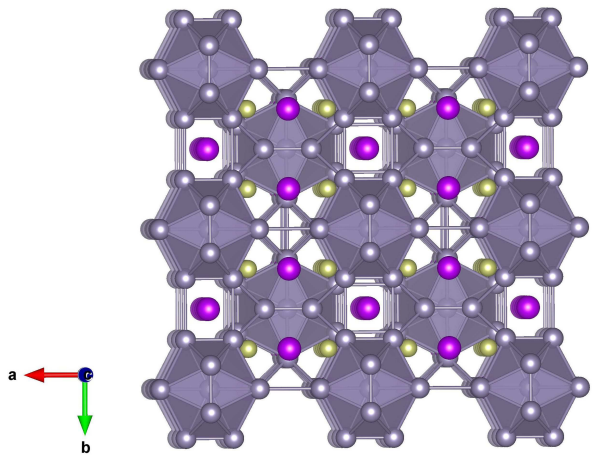

FIG. 1. (color online) The crystal structure of $Gd_3Ir_4Sn_{13}$ is depicted in the polyhedral coordination. The violet spheres are Gd, the yellow are Ir and the grey are Sn.

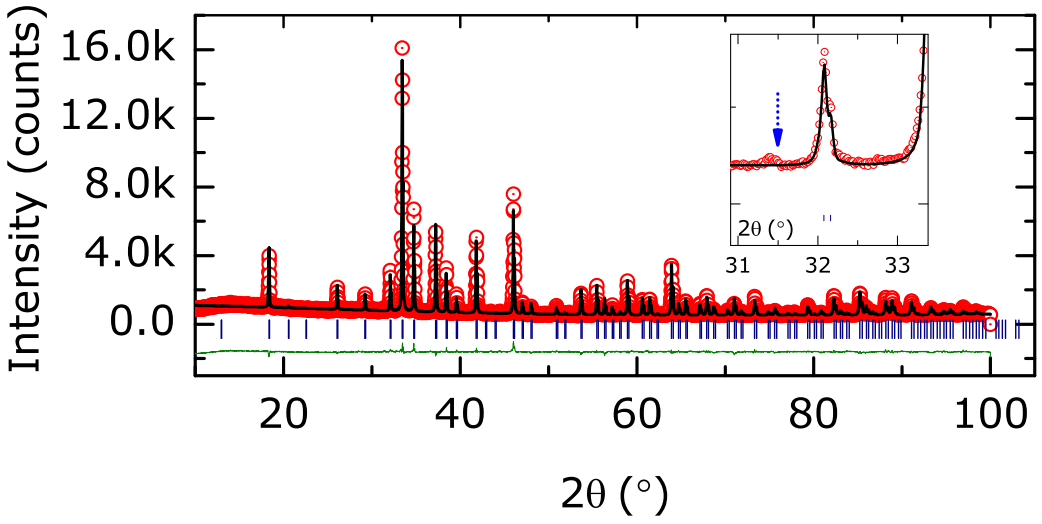

FIG. 2. (color online) The x ray diffraction pattern of $Gd_3Ir_4Sn_{13}$ is shown in red circles. The black solid line is the calculated pattern assuming $Pm\bar{3}n$ space group and the vertical bars are the allowed Bragg positions. The difference patterns is shown in green scatter. The inset of the graph highlights the region around $2\theta = 31.5^\circ$ where a superstructure peak is visible (the intensity axis is scaled down to show the feature clearly).

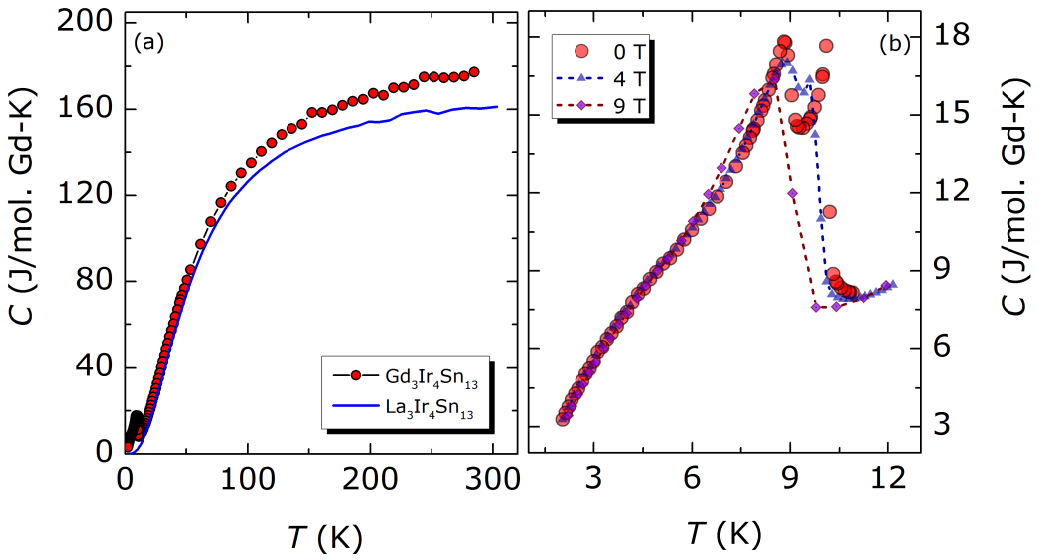

FIG. 3. (color online) (a) The experimentally measured specific heat of $Gd_3Ir_4Sn_{13}$ plotted in circles. The data for non-magnetic analogue $La_3Ir_4Sn_{13}$ plotted as a line. The double-phase transition occurring at $T_{N1} \approx 10$ K and $T_{N2} \approx 8.8$ K are shown magnified in (b) where the low-temperature specific heat in 0, 4 and 9 T are plotted together.

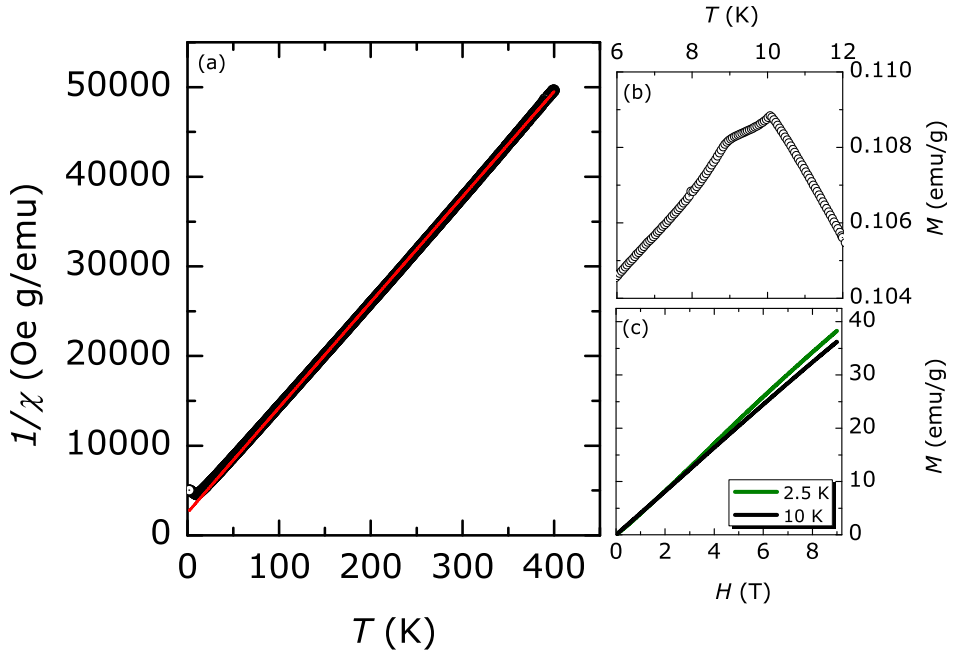

FIG. 4. (color online) (a) The inverse magnetic susceptibility $1/\chi(T)$ of $Gd_3Ir_4Sn_{13}$ plotted in circles along with the curve-fit using Curie-Weiss law shown as red solid line. (b) Shows the region of $M(T)$ displaying the double transitions at T_{N1} ≈10 K and $T_{N2} \approx$ 8.8 K. (c) Displays the magnetization isotherms at 2.5 K and 10 K which clearly shows the antiferromagnetic nature persisting up to 9 T.

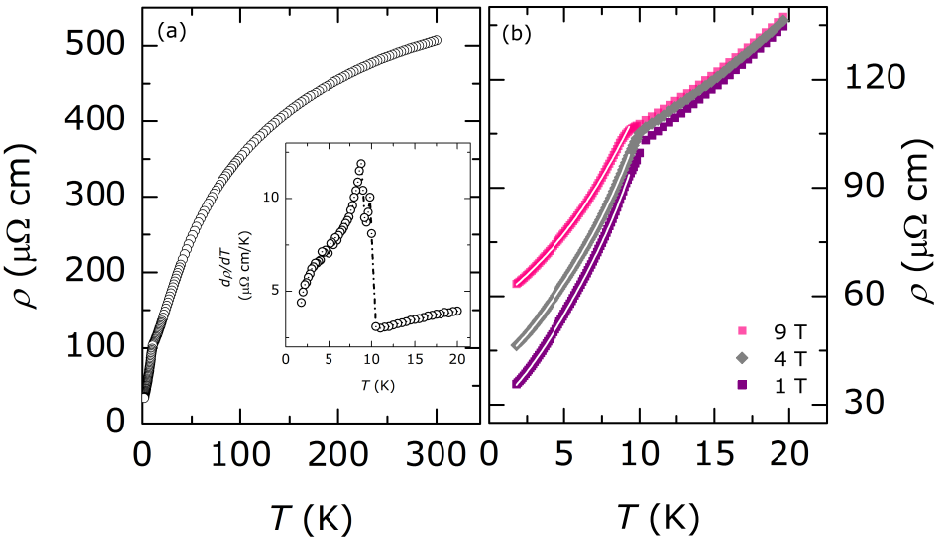

FIG. 5. (color online) (a) The electrical resistivity, $\rho(T)$, of $Gd_3Ir_4Sn_{13}$ in zero applied field. The derivative plot dρ/dT versus T is shown in the inset of (a). The double transitions are clearly observed in the derivative plot. Panel (b) shows the $\rho(T)$ obtained in applied fields 1, 4 and 9 T. The white solid lines are the curve fits according to Eqn (1).

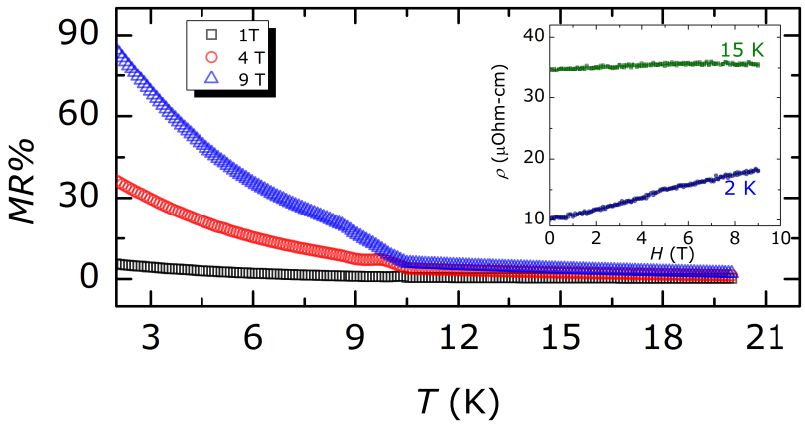

FIG. 6. (color online) The magnetoresistance, MR %, of $Gd_3Ir_4Sn_{13}$ for applied fields of 1, 4 and 9 T. The inset shows the isothermal magnetoresistance upto 9 T at 2 K as well as at 15 K. A giant, positive value of MR $\approx$ 80% is observed at 2 K upon the application of 9 T field.

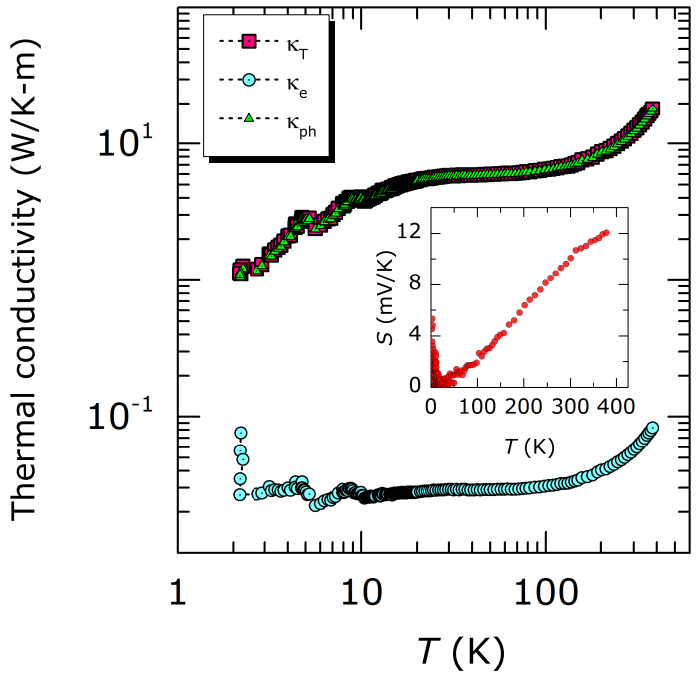

FIG. 7. (color online) The total thermal conductivity $\kappa_{\rm T}$ of $Gd_3Ir_4Sn_{13}$ is plotted along with the electronic ($\kappa_{\rm e}$) and the phonon contributions ($\kappa_{\rm ph}$). Notably, the double-transition is evident in the thermal transport data also. The inset shows the Seebeck coefficient.